

Emergence of intermediate range order in jammed packings

Joseph M. Monti,¹ Ishan Srivastava,² Leonardo E. Silbert,³
Andrew P. Santos,⁴ Jeremy B. Lechman,¹ and Gary S. Grest¹

¹*Sandia National Laboratories, Albuquerque, NM 87185, USA*

²*Center for Computational Sciences and Engineering,*

Lawrence Berkeley National Laboratory, Berkeley, California 94720, USA

³*School of Math, Science, and Engineering, Central New Mexico Community College, Albuquerque, New Mexico 87106, USA*

⁴*AMA Inc., Thermal Protection Materials Branch,*

NASA Ames Research Center, Moffett Field, CA 94035, USA

(Dated: October 24, 2024)

We perform a structural analysis of large scale jammed packings of monodisperse, frictionless and frictional spheres to elucidate structural signatures of the static structure factor in the low-to-intermediate wavenumber (q) region. We employ discrete element method simulations containing up to eighty million particles, in which the particle friction coefficient(s), including sliding, rolling, and twisting interactions, are varied. At intermediate q values, corresponding to length scales that lie between that of the nearest neighbor primary peak and the system size, we find the emergence of a prepeak—a signature of intermediate range order—that grows with increasing friction. We correlate the emergence of this peak to real space fluctuations in the local particle coordination number, which exhibits a grainy-like fluctuating field throughout the packing process that is retained in the final, mechanically stable state. While the formation of the prepeak shows varying degrees of robustness to packing protocol changes, our results suggest that preparation history may be used to construct packings with variable large length scale structural properties.

Mechanically stable packings of monodisperse spheres present as a model for studies of disordered, jammed systems. The macroscopic structure of frictionless jammed packings resembles those of other amorphous systems, such as glasses, inasmuch as there are traditional signatures of local structure. This is evinced by a primary, nearest neighbor peak readily seen in the static structure factor, $S(q)$, for wavenumbers q corresponding to the typical particle size, while at larger wavenumbers, $S(q)$ undergoes decaying oscillations that asymptote to unity [1]. For regular thermal systems, the small wavenumber limit of $S(q)$ relates to the mechanical properties of the system, i.e., $S(q \rightarrow 0) = S_0 = \rho k_B T \chi_T$, where ρ is the density of the system and χ_T is the isothermal susceptibility [2]. However, it is widely accepted that at longer wavelengths—larger length scales—jammed particle packings suppress density fluctuations compared to traditional liquid state theory, where a region of hyperuniformity persists, i.e., $S(q) \sim q$ [3–5].

An in-between scenario is also not uncommon in liquids and structural glasses, including colloidal systems [6]. At wavenumbers intermediate between the thermodynamic limit and the primary, nearest neighbor peak, evidence of structural correlations can sometimes emerge via the appearance of a prepeak: a feature in $S(q)$ that lies in the range $0 < q\sigma < 2\pi$, where σ represents the characteristic particle diameter. A prepeak in this q range signifies intermediate range order that is suggestive of a repeating motif spanning length scales of several, if not many, particle diameters. Intermediate range order has also been invoked as a controlling factor of packing efficiency and the dynamics in dense colloidal systems [7, 8].

While the general and superficial structural features between dense liquids and jammed packings share many

similarities [1, 9, 10], unlike liquids, static granular packings must satisfy not only global but also local conditions of mechanical stability. This results in constraints on both the mean particle coordination number and the local number of nearest neighbors with which individual particles directly interact. Such features are not usually qualified by typical averaging measures such as $S(q)$. Studies involving large scale packings potentially indicate fluctuations in the low q region of $S(q)$, suggesting the existence of hitherto unidentified features [4]. Such hints beg the question of whether additional structural organization does indeed exist within the jammed phase. It is precisely in this region of $S(q)$ where this work is focused. Here, we present static structure factor analyses that highlight the structural signatures in this intermediate range of length scales, for granular packings of frictionless and frictional particles using unprecedented large scale simulations of up to $\mathcal{O}(10^8)$ particles.

To address these questions, we perform three-dimensional discrete element method (DEM) simulations of spherical particles in LAMMPS [11]. Particles interact via frictional, damped, repulsive Hookean springs with spring constant k [12, 13], with rolling and twisting resistances modeled using Luding’s technique [14, 15]. The friction coefficients μ_s , μ_r , and μ_t set the sliding, rolling, and twisting resistances, respectively. Initial particle configurations are generated by randomly placing N particles with diameter σ [16] into a periodic cubic box with average particle density $\phi_0 = N\pi\sigma^3/6V_0$, where V_0 is the initial volume ($\phi_0 = 0.01$ unless otherwise stated). Particle overlaps in the starting configurations are relaxed by running constant volume dynamics with viscous damping until the kinetic energy vanishes. Mechanically stable jammed packings are created by ap-

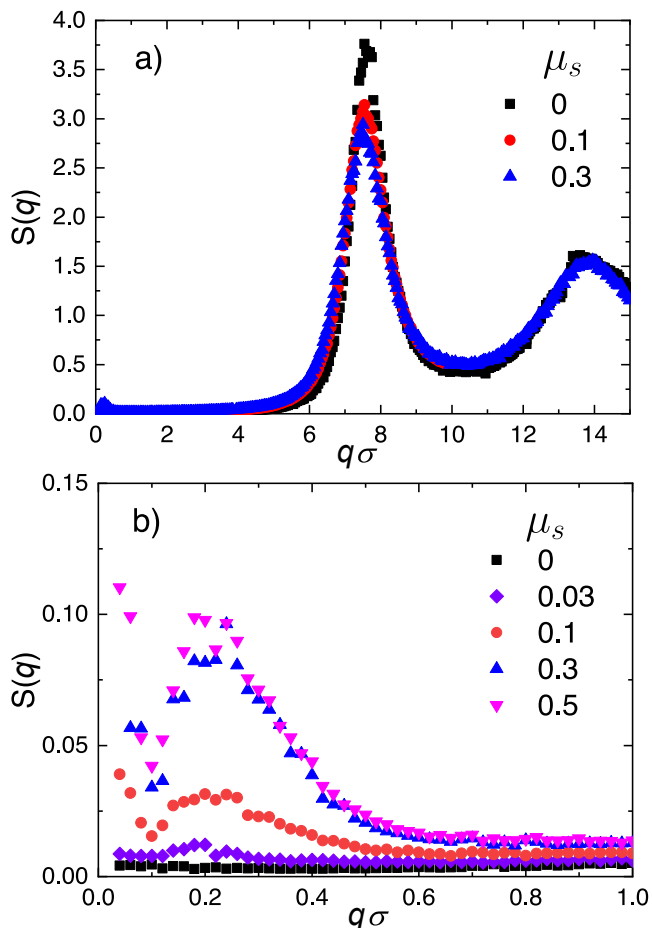


FIG. 1. (a) Static structure factor $S(q)$ for packings with $N = 10^6$ particles at the indicated values of the sliding friction coefficient μ_s . (b) $S(q)$ at low q for packings with $N = 10^7$ particles over a broader range of sliding friction coefficients μ_s . The associated ϕ values for increasing μ_s in b) are: 0.638, 0.624, 0.611, 0.595, 0.590, respectively.

plying a small hydrostatic pressure P to contract the volume using the isobaric-isoenthalpic (NPH) ensemble, with $P\sigma/k = 10^{-5}$ to probe the hard-particle limit of jamming; other simulation parameters closely follow Santos *et al.* [15]. The simulations proceed until the internal and applied stress tensors match and the kinetic energy per particle is small, typically $\mathcal{O}(10^{-12})$ or less. The final jammed simulation boxes are triclinic with small tilt values on the order of σ . Calculation of $S(q)$ for triclinic boxes is accomplished following Monti *et al.* [17].

Most features of the static structure factor for frictionless, monodisperse systems are understood—e.g., the positions and amplitudes of the primary and higher order peaks, and the $q \rightarrow \infty$ asymptotic behavior [1, 3, 4]. Figure 1a shows $S(q)$ for frictionless and frictional particle packings with $N = 10^6$ particles; the salient effect of inter-particle friction is to diminish the primary peak as the particle coordination number is reduced [15]. The corresponding volume fractions range from $\phi = 0.639$ for $\mu_s = 0$ to $\phi = 0.594$ for $\mu_s = 0.3$. We intend to focus on

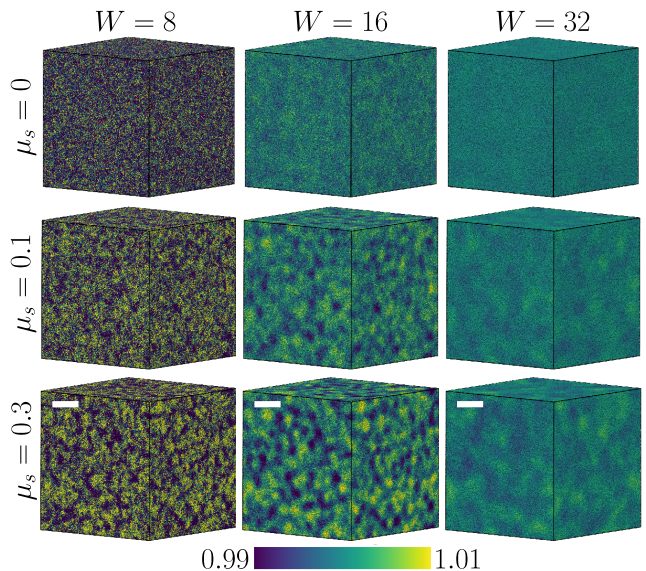


FIG. 2. Visualizations of the variation of particle coordination evaluated over a spherical window with diameter $W\sigma$, normalized by the coordination expected assuming uniform particle density, for three values of μ_s . The color bar indicates coordination variations of $\pm 1\%$. Each packing contains $N = 10^7$ particles, with the characteristic simulation length $\sim V^{1/3} \sim 200\sigma$. The superposed scale bar in the final row of images corresponds to 50σ . The images were rendered in OVITO [20].

the role of friction in introducing structure on intermediate scales, i.e., on scales much larger than σ and much smaller than the characteristic simulation length $\sim V^{1/3}$. Figure 1b magnifies the low q region for varying μ_s and reveals the emergence of a prepeak spanning a range of q loosely corresponding to length scales of $10\sigma - 60\sigma$, at its broadest. $S(q)$ for frictionless, athermal packings has universally been found to increase monotonically with q in this regime [1, 3, 5, 10, 18]; conversely, we highlight here that the prepeak for even a modest amount of sliding friction is distinguishable from frictionless data at similar q , despite only small changes to global packing metrics such as ϕ or the mean coordination number with nonzero friction [15]. The amplitude of the prepeak grows quickly with increasing μ_s before saturating for $\mu_s \geq 0.3$, beyond which additional sliding friction has limited impact [19].

Structure over intermediate length scales can be demonstrated visually by quantifying variations of particle density. Figure 2 depicts fluctuations in the number of neighbors (coordination number) contained within a spherical window with diameter $W\sigma$ centered on each particle, normalized by the number of neighbors expected assuming the density within the window is ϕW^3 [3]. This strategy picks out density variations on scales comparable to $W\sigma$, which manifest in $S(q)$ as peaks at $q\sigma \sim 2\pi/W$. Considering $8 \leq W \leq 32$, the images indicate that frictionless packings exhibit no marked density fluctuations over these length scales, whereas frictional packings show characteristic structure on scales much larger than σ , an

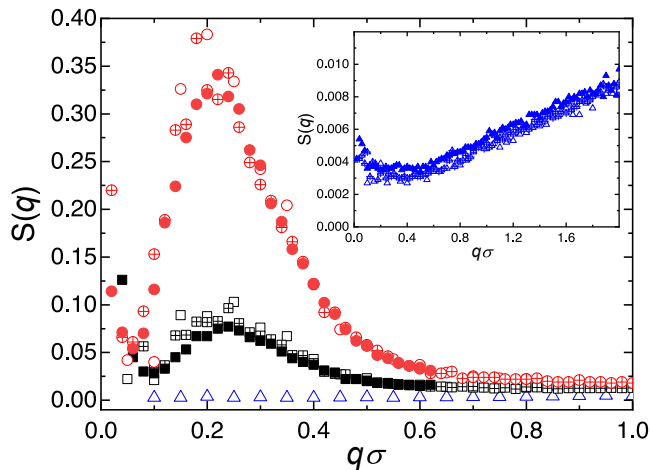


FIG. 3. $S(q)$ computed for packings with $N = 10^6$ (open), 10^7 (hatched), and 8×10^7 (filled symbols) for $\{\mu_s, \mu_r, \mu_t\}$: $\{0, 0, 0\}$ (blue), $\{0.3, 0, 0\}$ (black), and $\{0.3, 0.3, 0.3\}$ (red). Inset: $S(q)$ for frictionless systems with symbols matching those in the main figure.

effect that grows more prominent with increasing friction. This range of window sizes corresponds to the upper half of wavenumbers where the prepeak is apparent in Fig. 1b, and is much smaller than the simulation length $V^{1/3} \sim 200\sigma$.

The effect of strengthening frictional interactions by including rolling and twisting resistances between particles is shown in Fig. 3. For $\mu_s = \mu_r = \mu_t = 0.3$ ($\phi = 0.572$ for $N = 10^7$), the prepeak spans a broader range of q and more than triples in magnitude compared to the case with only sliding friction, though the peak maxima occur at nearly identical q . The prepeak extending to larger q suggests that packings with all friction modes active can support enhanced structure over shorter length scales—i.e., density fluctuations spread over fewer particle diameters—compared to packings stabilized solely by sliding friction. Figure 3 also demonstrates that the prepeak is independent of system size (provided the system is sufficiently large). Note that each increase in N in the figure roughly halves the minimum accessible nonzero q and drastically increases the number of wavenumbers comprising the prepeak. Thus, the prepeak is not an artifact of the simulation interacting with its periodic images; however, we cannot rule out periodicity effects causing the upturn of $S(q)$ for the smallest $q\sigma \sim 2\pi\sigma/V^{1/3}$.

The inset of Fig. 3 shows results for $S(q)$ for frictionless packings for systems up to size $N = 8 \times 10^7$ (with $\phi = 0.638$). As found previously [3–5], $S(q)$ shows a linear relationship, i.e., $S(q) = A + Bq$, for intermediate wavenumbers. The intercept $A \approx 0.002$ is slightly larger than the earlier works reported, possibly owing to differing packing protocols. As observed by Ikeda *et al.* [5], for $q \lesssim 0.35\sigma^{-1}$ a distinctive upturn in $S(q)$ is observed for the larger systems. Whether this upturn corresponds to the beginnings of a peak at very low q , similar to our

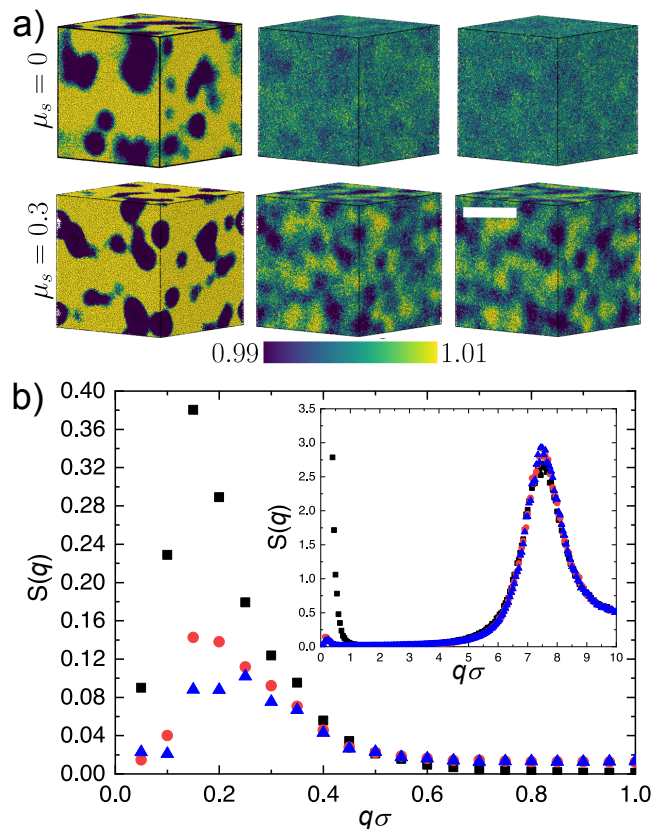


FIG. 4. (a) Visualizations of normalized coordination fluctuations evaluated with $W = 8$ for systems with $N = 10^6$ particles at the indicated values of μ_s . The first two visualizations occur at 1×10^5 and 2×10^5 time steps, and the final configurations at 6.6×10^7 time steps for $\mu_s = 0$ and 8×10^6 time steps for $\mu_s = 0.3$. For each image, $V^{1/3} \sim 96\sigma$ and the scale bar in the final image indicates 50σ . (b) $S(q)$ at low q for the $\mu_s = 0.3$ configurations depicted in (a), shown in ascending order of simulation time as black squares, red circles, and blue triangles. The earliest simulation time data (black squares) are scaled by a factor of 0.02 to facilitate comparison of the low q ranges. Inset: unscaled $S(q)$ over a larger range of q .

findings for frictional particles, is an open question.

The formation of the intermediate structure responsible for the prepeak is apparent through examining a time sequence of packing configurations. Figure 4a shows coordination variations for early, later, and final configurations for frictionless and frictional particles, both of which begin from the same dilute initial state. The visualization scheme ($W = 8$) highlights large coordination variations that form over the first 1×10^5 time steps of consolidation (from $\phi_0 = 0.01$ to $\phi \approx 0.600$ and 0.572 for frictionless and frictional, respectively), but at 2×10^5 time steps it is clear that the frictionless system anneals out the early-time structure, while the variations are more resilient in frictional systems. Moreover, the second and third images appear similar for each case, implying that local particle rearrangements during the latter pack-

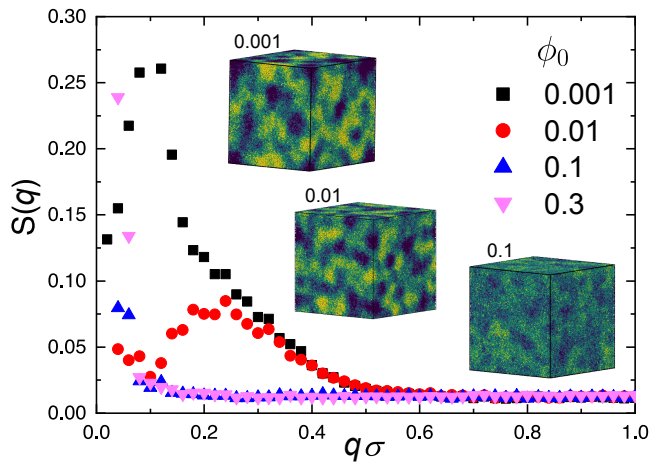


FIG. 5. $S(q)$ at low q for packings with the indicated values of initial volume fraction ϕ_0 for a system of $N = 1 \times 10^7$ particles with $\mu_s = 0.3$. Snapshots of several of the corresponding normalized coordination fluctuations for $N = 1 \times 10^6$, evaluated with $W = 8$ are included. Particle coloration is identical to Fig. 4a.

ing stages ($\phi \approx 0.629 \rightarrow 0.639$ and $0.593 \rightarrow 0.594$) do not disrupt the intermediate structure.

To quantify these observations, $S(q)$ for the frictional configurations of Fig. 4a are shown in Fig. 4b. After 1×10^5 time steps, the prepeak is present over roughly the same q -range as in the final configuration, albeit with a much large amplitude; to facilitate comparison with later times, the prepeak at 1×10^5 time steps is scaled by 0.02 in the main figure, while the inset plots the unscaled data, demonstrating that the prepeak is initially comparable to the primary neighbor peak in magnitude. Between 2×10^5 time steps and the final configuration, there is a slight reduction and shift of the prepeak, implying that the structure is essentially locked in at early packing stages.

The intermediate structure exhibited above is dependent on both initial configuration and packing protocol. Focusing on the role of initial density, Fig. 5 compares $S(q)$ for small q and coordination variation images for a range of ϕ_0 . Final packing volume fractions for $\phi_0 = 0.001$ and 0.1 are similar to $\phi_0 = 0.01$, with $\phi \approx 0.595$, whereas the $\phi_0 = 0.3$ system packs more loosely to $\phi = 0.590$. Compared to $\phi_0 = 0.01$, the prepeak for $\phi_0 = 0.001$ is amplified and shifted to lower q (larger length scale). Packings starting with $\phi_0 = 0.1$ and 0.3 do not exhibit a prepeak over intermediate length scales, while their $S(q)$ do show strong peaks at the lowest nonzero q . The dichotomy across ϕ_0 helps explain the physical origin of the density fluctuations: starting from a dilute, randomized state, volumetric contraction towards a central point produces both clumps of particles and depleted regions. Higher density initial configurations do not contract as far and so are less clumpy at the outset, and have stronger correlations between particle positions arising from the overlap-removing procedure we perform.

Indeed, the radial distribution functions for the initial configurations (not shown) reveal no pronounced liquid-like ordering for $\phi_0 = 0.001$ and 0.01 , but a clear contact peak forms for $\phi_0 = 0.1$ and additional secondary structure appears for $\phi_0 = 0.3$. Among other factors, including kinetic energy introduced during packing, the degree of homogeneity at early stages may play an important role in producing intermediate structure.

Protocol dependence in frictional, non-cohesive granular materials is well known [21–29]. We found that the intermediate structure described in this work could be reduced or eliminated through several means, including: adding a strong damping contribution to the barostat (modifying the Nosé-Hoover formalism); over-compressing the packing at higher P before reducing to the nominal P ; or, employing the Berendsen barostat [30] as an alternative. Raising P by one or two orders of magnitude while maintaining our original packing strategy did not entirely remove the prepeak. It is also conceivable that volume-controlled packing strategies will suppress the fragile structures that produce the prepeak, considering the challenges they pose for jamming particles at low pressures [29, 31], although we did not test this supposition here.

To summarize, static structure factor calculations for large jammed packings of frictional monodisperse spheres identified unexpected structure at intermediate length scales of order 10 to 60 times the particle diameter. The intermediate structure was absent for packings of frictionless particles, which instead displayed linear behavior over a limited range of wavenumbers with an upturn at the lowest q , consistent with other recent studies. Investigation into the origin of the many-particle structures revealed that pronounced particle density fluctuations at early packing stages were responsible for the intermediate structure. Additional tests suggested that packing protocol and initial conditions are crucial for preserving the intermediate order in the jammed configurations. Nevertheless, the results show that athermal, mechanically stable packing states can support heterogeneous structure over a range of length scales not restricted to the immediate neighborhood around each particle.

I.S. acknowledges support from the U.S. Department of Energy (DOE), Office of Science, Office of Advanced Scientific Computing Research, Applied Mathematics Program under Contract No. DE-AC02-05CH11231. This work was performed in part at the Center for Integrated Nanotechnologies, a U.S. DOE and Office of Basic Energy Sciences user facility. Sandia National Laboratories is a multimission laboratory managed and operated by National Technology & Engineering Solutions of Sandia, LLC, a wholly owned subsidiary of Honeywell International Inc., for the U.S. DOE’s National Nuclear Security Administration under contract DE-NA0003525. This paper describes objective technical results and analysis. Any subjective views or opinions that might be expressed in the paper do not necessarily represent the views of the U.S. DOE or the U.S. Government.

-
- [1] C. S. O’Hern, L. E. Silbert, A. J. Liu, and S. R. Nagel, *Phys. Rev. E* **68**, 011306 (2003).
- [2] J.-P. Hansen and I. R. McDonald, *Theory of Simple Liquids*, 4th ed. (Academic Press, Oxford, 2013).
- [3] A. Donev, F. H. Stillinger, and S. Torquato, *Phys. Rev. Lett.* **95**, 090604 (2005).
- [4] L. E. Silbert and M. Silbert, *Phys. Rev. E* **80**, 041304 (2009).
- [5] A. Ikeda, L. Berthier, and G. Parisi, *Phys. Rev. E* **95**, 052125 (2017).
- [6] D. L. Price, S. C. Moss, R. Reijers, M. L. Saboungi, and S. Susman, *J. Phys.: Cond. Matt.* **1**, 1005 (1989).
- [7] H. Yuan, Z. Zhang, W. Kob, and Y. Wang, *Phys. Rev. Lett.* **127**, 278001 (2021).
- [8] N. Singh, Z. Zhang, A. K. Sood, W. Kob, and R. Ganapathy, *PNAS* **120**, e2300923120 (2023).
- [9] R. D. Kamien and A. J. Liu, *Phys. Rev. Lett.* **99**, 155501 (2007).
- [10] A. Ikeda and L. Berthier, *Phys. Rev. E* **92**, 012309 (2015).
- [11] A. P. Thompson, H. M. Aktulga, R. Berger, D. S. Bolintineanu, W. M. Brown, P. S. Crozier, P. J. in ’t Veld, A. Kohlmeyer, S. G. Moore, T. D. Nguyen, R. Shan, M. J. Stevens, J. Tranchida, C. Trott, and S. J. Plimpton, *Comput. Phys. Comm.* **271**, 108171 (2022).
- [12] P. A. Cundall and O. D. L. Strack, *Géotechnique* **29**, 47 (1979).
- [13] L. E. Silbert, D. Ertas, G. S. Grest, T. C. Halsey, D. Levine, and S. J. Plimpton, *Phys. Rev. E* **64**, 051302 (2001).
- [14] S. Luding, *Gran. Matt.* **10**, 235–246 (2008).
- [15] A. P. Santos, D. S. Bolintineanu, G. S. Grest, J. B. Lechman, S. J. Plimpton, I. Srivastava, and L. E. Silbert, *Phys. Rev. E* **102**, 032903 (2020).
- [16] We found that introducing $\pm 5\%$ diameter dispersity did not change the results.
- [17] J. M. Monti, I. Srivastava, L. E. Silbert, J. B. Lechman, and G. S. Grest, *Phys. Rev. E* **108**, L042902 (2023).
- [18] C. E. Maher, Y. Jiao, and S. Torquato, *Phys. Rev. E* **108**, 1 (2023).
- [19] L. E. Silbert, D. Ertas, G. S. Grest, T. C. Halsey, and D. Levine, *Phys. Rev. E* **65**, 031304 (2002).
- [20] A. Stukowski, *Modell. Simul. Mater. Sci. Eng.* **18**, 015012 (2009).
- [21] E. Nowak, J. Knight, M. Povinelli, H. Jaeger, and S. Nagel, *Powd. Tech.* **94**, 79 (1997).
- [22] A. Santomaso, P. Lazzaro, and P. Canu, *Chem. Eng. Sci.* **58**, 2857 (2003).
- [23] J. W. Landry, G. S. Grest, L. E. Silbert, and S. J. Plimpton, *Phys. Rev. E* **67**, 041303 (2003).
- [24] E. Somfai, M. van Hecke, W. G. Ellenbroek, K. Shundyak, and W. van Saarloos, *Phys. Rev. E* **75**, 020301 (2007).
- [25] C. Song, P. Wang, and H. A. Makse, *Nature* **453**, 629 (2008).
- [26] S. Dagois-Bohy, B. P. Tighe, J. Simon, S. Henkes, and M. van Hecke, *Phys. Rev. Lett.* **109**, 095703 (2012).
- [27] E. S. Billighn, J. E. Kollmer, and K. E. Daniels, *Phys. Rev. Lett.* **122**, 038001 (2019).
- [28] S. Luding, *Nature Physics* **12**, 531 (2016).
- [29] A. P. Santos, I. Srivastava, L. E. Silbert, J. B. Lechman, and G. S. Grest, *Frontiers Soft Matter* **3**, 1 (2024).
- [30] H. J. C. Berendsen, J. P. M. Postma, W. F. van Gunsteren, A. DiNola, and J. R. Haak, *The Journal of Chemical Physics* **81**, 3684 (1984).
- [31] L. E. Silbert, *Soft Matter* **6**, 2918 (2010).